

## Astrophysical Implications of the $^{139}\text{La}(n,\gamma)$ and $^{151}\text{Sm}(n,\gamma)$ Cross Section Measured at n\_TOF

S. Marrone<sup>\* 19</sup>, U. Abbondanno<sup>20</sup>, G. Aerts<sup>7</sup>, H. Álvarez<sup>35</sup>, F. Alvarez-Velarde<sup>31</sup>, S. Andriamonje<sup>7</sup>, J. Andrzejewski<sup>26</sup>, P. Assimakopoulos<sup>16</sup>, L. Audouin<sup>12</sup>, G. Badurek<sup>1</sup>, P. Baumann<sup>10</sup>, F. Bečvář<sup>6</sup>, E. Berthoumieux<sup>7</sup>, F. Calviño<sup>34</sup>, D. Cano-Ott<sup>31</sup>, R. Capote<sup>3,36</sup>, C. Carrapiço<sup>27</sup>, P. Cennini<sup>37</sup>, V. Chepel<sup>28</sup>, E. Chiaveri<sup>37</sup>, N. Colonna<sup>19</sup>, G. Cortes<sup>33</sup>, A. Couture<sup>41</sup>, J. Cox<sup>41</sup>, M. Dahlfors<sup>37</sup>, S. David<sup>9</sup>, I. Dillmann<sup>12</sup>, R. Dolfini<sup>23</sup>, C. Domingo-Pardo<sup>32</sup>, W. Dridi<sup>7</sup>, I. Duran<sup>35</sup>, C. Eleftheriadis<sup>13</sup>, M. Embid-Segura<sup>31</sup>, L. Ferrant<sup>9</sup>, A. Ferrari<sup>37</sup>, R. Ferreira-Marques<sup>28</sup>, L. Fitzpatrick<sup>37</sup>, H. Fraiss-Koelbl<sup>3</sup>, K. Fujii<sup>20</sup>, W. Furman<sup>30</sup>, R. Gallino<sup>22</sup>, I. Goncalves<sup>28</sup>, E. Gonzalez-Romero<sup>31</sup>, A. Goverdovski<sup>29</sup>, F. Gramegna<sup>18</sup>, E. Griesmayer<sup>3</sup>, C. Guerrero<sup>31</sup>, F. Gunsing<sup>7</sup>, B. Haas<sup>8</sup>, R. Haight<sup>39</sup>, M. Heil<sup>12</sup>, A. Herrera-Martinez<sup>37</sup>, M. Igashira<sup>25</sup>, S. Isaev<sup>9</sup>, E. Jericha<sup>1</sup>, Y. Kadi<sup>37</sup>, F. Käppeler<sup>12</sup>, D. Karamanis<sup>16</sup>, D. Karadimos<sup>16</sup>, M. Kerveno<sup>10</sup>, V. Ketlerov<sup>29,37</sup>, P. Koehler<sup>40</sup>, V. Konovalov<sup>30,37</sup>, E. Kossionides<sup>15</sup>, M. Krtička<sup>6</sup>, C. Lamboudis<sup>13</sup>, H. Leeb<sup>1</sup>, A. Lindote<sup>28</sup>, I. Lopes<sup>28</sup>, M. Lozano<sup>36</sup>, S. Lukic<sup>10</sup>, J. Marganec<sup>26</sup>, P. Mastinu<sup>18</sup>, A. Mengoni<sup>3,37</sup>, P.M. Milazzo<sup>20</sup>, C. Moreau<sup>20</sup>, M. Mosconi<sup>12</sup>, F. Neves<sup>28</sup>, H. Oberhummer<sup>1</sup>, S. O'Brien<sup>41</sup>, M. Oshima<sup>24</sup>, J. Pancin<sup>7</sup>, C. Papachristodoulou<sup>16</sup>, C. Papadopoulos<sup>14</sup>, C. Paradela<sup>35</sup>, N. Patronis<sup>16</sup>, A. Pavlik<sup>2</sup>, P. Pavlopoulos<sup>11</sup>, L. Perrot<sup>7</sup>, M. Pignatari<sup>22</sup>, R. Plag<sup>12</sup>, A. Plompen<sup>5</sup>, A. Plukis<sup>7</sup>, A. Poch<sup>33</sup>, C. Pretel<sup>33</sup>, J. Quesada<sup>36</sup>, T. Rauscher<sup>38</sup>, R. Reifarth<sup>39</sup>, M. Rosetti<sup>17</sup>, C. Rubbia<sup>23</sup>, G. Rudolf<sup>10</sup>, P. Rullhusen<sup>5</sup>, J. Salgado<sup>27</sup>, L. Sarchiapone<sup>37</sup>, I. Savvidis<sup>13</sup>, C. Stephan<sup>9</sup>, G. Tagliente<sup>19</sup>, J.L. Tain<sup>32</sup>, L. Tassan-Got<sup>9</sup>, L. Tavora<sup>27</sup>, R. Terlizzi<sup>19</sup>, G. Vannini<sup>21</sup>, P. Vaz<sup>27</sup>, A. Ventura<sup>17</sup>, D. Villamarin<sup>31</sup>, M.C. Vincente<sup>31</sup>, V. Vlachoudis<sup>37</sup>, R. Vlastou<sup>14</sup>, F. Voss<sup>12</sup>, S. Walter<sup>12</sup>, H. Wendler<sup>37</sup>, M. Wiescher<sup>41</sup>, K. Wisshak<sup>12</sup>

<sup>1</sup>Atominstytut der Österreichischen Universitäten, Technische Universität Wien, Austria,

<sup>2</sup>Institut für Isotopenforschung und Kernphysik, Universität Wien, Austria,

<sup>3</sup>International Atomic Energy Agency, NAPC-Nuclear Data Section, Vienna, Austria

<sup>4</sup>Fachhochschule Wiener Neustadt, Wiener Neustadt, Austria,

<sup>5</sup>CEC-JRC-IRMM, Geel, Belgium,

<sup>6</sup>Charles University, Prague, Czech Republic,

<sup>7</sup>CEA/Saclay - DSM, Gif-sur-Yvette, France,

<sup>8</sup>Centre National de la Recherche Scientifique/IN2P3 - CENBG, Bordeaux, France,

<sup>9</sup>Centre National de la Recherche Scientifique/IN2P3 - IPN, Orsay, France,

<sup>10</sup>Centre National de la Recherche Scientifique/IN2P3 - IReS, Strasbourg, France,

<sup>11</sup>Pôle Universitaire Léonard de Vinci, Paris La Défense, France,

<sup>12</sup>Forschungszentrum Karlsruhe GmbH (FZK), Institut für Kernphysik, Germany,

<sup>13</sup>Aristotle University of Thessaloniki, Greece,

<sup>14</sup>National Technical University of Athens, Greece,

<sup>15</sup>NCSR, Athens, Greece,

<sup>16</sup>University of Ioannina, Greece,

<sup>17</sup>ENEA, Bologna, Italy,

<sup>18</sup>Istituto Nazionale di Fisica Nucleare (INFN), Laboratori Nazionali di Legnaro, Italy,

<sup>19</sup>Dipartimento di Fisica and Istituto Nazionale di Fisica Nucleare, Bari, Italy,

<sup>20</sup>Istituto Nazionale di Fisica Nucleare, Trieste, Italy,

<sup>21</sup>Dipartimento di Fisica, Università di Bologna, and Sezione INFN di Bologna, Italy,

\* Speaker and corresponding author, address: via Orabona 4, 70125 Bari (Italy). Tel. +390805442511, e-mail stefano.marrone@ba.infn.it .

- <sup>22</sup>Dipartimento di Fisica, Università di Torino and Sezione INFN di Torino, Italy,  
<sup>23</sup>Università degli Studi Pavia, Pavia, Italy,  
<sup>24</sup>Japan Atomic Energy Research Institute, Tokai-mura, Japan,  
<sup>25</sup>Tokyo Institute of Technology, Tokyo, Japan,  
<sup>26</sup>University of Lodz, Lodz, Poland  
<sup>27</sup>Instituto Tecnológico e Nuclear (ITN), Lisbon, Portugal,  
<sup>28</sup>LIP - Coimbra & Departamento de Física da Universidade de Coimbra, Portugal,  
<sup>29</sup>Institute of Physics and Power Engineering, Kaluga region, Obninsk, Russia,  
<sup>30</sup>Joint Institute for Nuclear Research, Dubna, Russia,  
<sup>31</sup>CIEMAT, Madrid, Spain,  
<sup>32</sup>Istituto de Física Corpuscular, CSIC-Universidad de Valencia, Spain,  
<sup>33</sup>Universitat Politècnica de Catalunya, Barcelona, Spain,  
<sup>34</sup>Universidad Politécnica de Madrid, Spain,  
<sup>35</sup>Universidade de Santiago de Compostela, Spain,  
<sup>36</sup>Universidad de Sevilla, Spain,  
<sup>37</sup>CERN, Geneva, Switzerland,  
<sup>38</sup>Department of Physics and Astronomy - University of Basel, Basel, Switzerland,  
<sup>39</sup>Los Alamos National Laboratory, New Mexico, USA,  
<sup>40</sup>Oak Ridge National Laboratory, Physics Division, Oak Ridge, USA,  
<sup>41</sup>University of Notre Dame, Notre Dame, USA.

The nuclear resonance parameters and the capture cross section of the neutron magic isotope  $^{139}\text{La}$  and of the radioactive isotope  $^{151}\text{Sm}$  have been measured relative to  $^{197}\text{Au}$  in the energy range of 0.6 eV-1 MeV at neutron time-of-flight (n\_TOF) facility at CERN. The description of the experimental apparatus is followed by the presentation of the data analysis procedures consisting in the efficiency correction by means of the Pulse Height Weighting Function technique, in the determination of different background components and in their subtraction. We extracted the resonance parameters and the related nuclear quantities such as the resonance integral, the average gamma width, the nuclear level densities and the neutron strength function. These results improve the accuracy of the existing data. The deduced values of the Maxwellian-averaged capture cross section, together with the most recent spectroscopic observations in low metallicity stars, provide key indications for modelling the nucleosynthesis and the chemical evolution of heavy nuclei in the Galaxy.

*International Symposium on Nuclear Astrophysics – Nuclei in the Cosmos – IX*  
 CERN, Geneva, Switzerland  
 25-30 June, 2006

## 1. Introduction

Lanthanum and samarium assume a relevant role in nuclear astrophysics.  $^{139}\text{La}$  is a neutron magic isotope that belongs to the second *slow* neutron capture process (Ba to Nd). Consequently, it is particularly suited for monitoring the heavy *s*-process abundances from Ba up to Pb. Moreover, solar lanthanum is almost monoisotopic, being composed of  $^{139}\text{La}$  for 99.91% and it is relatively easy to observe in stellar spectra.

The  $^{151}\text{Sm}$  is one of the main branch point isotopes in the *s* process. The competition between neutron capture and  $\beta$ -decay leads to a split of the reaction path at  $^{151}\text{Sm}$  followed by a second branching at  $^{154}\text{Eu}$ . While the additional branch points  $^{152}, ^{155}\text{Eu}$  and  $^{153}\text{Gd}$  are of minor importance, the branchings at  $^{151}\text{Sm}$  and  $^{154}\text{Eu}$  determine the abundances of the *s*-only isotopes  $^{152}\text{Gd}$  and  $^{154}\text{Gd}$ , respectively. Since the  $\beta$ -decay rate of  $^{151}\text{Sm}$  depends on temperature this branching can be used to extract important information on the thermodynamic conditions during the *s* process from the local abundance pattern in this mass range [1].

Since the  $^{151}\text{Sm}$  is radioactive, the previous experimental data were derived long time ago from transmission measurements by Pattenden [2] and by Kirouac and Eiland [3]. The  $^{139}\text{La}(n,\gamma)$  cross section has been measured at Oak Ridge [4] and JAERI [5] while a transmission measurement was performed several years ago at the Columbia University synchrotron [6]. In order to improve the accuracy of those data and to satisfy the various requests, those capture measurements have been performed in a wide energy range at the innovative neutron time-of-flight facility (n\_TOF) at CERN laboratories.

## 2. Experimental Set-up and Data Analysis

The neutron beam at n\_TOF is produced by spallation of a 20 GeV/c proton beam from the CERN proton synchrotron onto a massive natural Pb target. The characteristics of the proton and the neutron beam are extensively illustrated in Ref. [7]. The set-up for the capture measurements consists of a low-mass neutron flux monitoring system based on silicon detectors used for the relative normalization of the spectra taken with the different samples under investigation [8], and two  $\text{C}_6\text{D}_6$  scintillators which detect the capture  $\gamma$ -rays. The  $\text{C}_6\text{D}_6$  used in the present measurement consisted of cylindrical cells 127.3 mm in diameter and 78 mm in length with an active volume of  $\sim 1000\text{ cm}^3$ . The low neutron sensitivity of the  $\text{C}_6\text{D}_6$  was further minimized by coupling a thin carbon fiber cell directly to the EMI 9823QKA photomultipliers [9]. The innovative data acquisition system is based on fast digitizers, which records the full analogue waveform of the detector signal during the entire transit time of the neutron burst [10]. These signals are analyzed off-line by determining the corresponding information on TOF, charge, amplitude, and particle type [11]. Finally in Ref. [7], the characteristics (mass, dimensions and composition) of all samples and particularly of  $\text{Sm}_2\text{O}_3$  are listed. It has to be noticed that the  $\text{Sm}_2\text{O}_3$  sample contains several impurities of other samarium isotopes and of the  $^{152}\text{Eu}$  ( $\beta$ -decay product of  $^{151}\text{Sm}$ ).

The efficiency correction is based on the Pulse Height Weighting Function technique (PHWT). The PHWT [12] consists of modifying by software the detector response  $R(E_n, E_D)$ , being  $E_n$  the neutron energy and  $E_D$  the energy deposited in the scintillator, so that the detection efficiency does not depend on the details of the cascade but only on the total capture energy. In order to calculate the weighting function necessary for such modification, different sets of Monte Carlo simulations using the GEANT-3.21, GEANT-4 and MCNP packages were performed. The geometry and materials of the experimental set-up were carefully implemented and the distribution of the photon source points was assumed uniform in depth and gaussian in profile. From the simulated response distributions, the weighting functions, parameterized with a fourth degree polynomial, are obtained by the least square method (see Eq. 3 in Ref. [12]).

In order to perform accurate measurements of the cross section, a careful evaluation of the background is needed. In general, neutron capture measurements at n\_TOF are affected by essentially three different sources of background: neutrons scattered by the sample, in-beam  $\gamma$ -rays, and the ambient background. The ambient background is mostly generated by particles from the spallation target, which have passed the shieldings and the sweeping magnet. In the present case, an additional component, common to all samples and proportional only to the integrated neutron fluence, is caused by the cans of the samples (Aluminum for the  $^{139}\text{La}$  and Titanium for the  $^{151}\text{Sm}$ ). The background related to neutrons scattered by the sample and captured in the walls of the experimental area, in the detectors, or in surrounding materials, was investigated by means of a natural carbon sample that was chosen to match the elastic scattering effect of the  $\text{Sm}_2\text{O}_3$  sample. The effect of scattered neutrons was negligible because of the very low neutron sensitivity of the set-up (e.g. the carbon-fiber) and because materials with large capture cross sections had been completely removed from the experimental area. Finally a quantitative estimate of the in-beam  $\gamma$ -background for each sample is obtained scaling the contribution measured with a Pb sample, complemented by a detailed Monte Carlo simulation of the interaction of the in-beam  $\gamma$ -rays with the sample under study. The resulting yield distribution is scaled by the normalization factor  $k_\gamma$  extracted from the simulations and then subtracted to the raw spectra of each sample. Finally minor corrections are also performed on the subtracted spectra through the estimations of several effects like: self-shielding, multiple scattering, Doppler broadening and the neutron beam resolution.

### 3. Results and Implications

The capture cross section of  $^{139}\text{La}$  is measured up to 9 keV and is expressed in terms of  $R$ -matrix resonance parameters calculated in the Reich-Moore approximation by mean of the code SAMMY. The fit of the resonances is performed in different ways in order to check the reliability of the extracted parameters. The main step of the fitting procedure consisted in the extraction of the resonance parameters from the background-subtracted capture yields. The spin assignment of each level is carefully checked comparing the fitting results of the different assignments listed in the various nuclear data libraries: ENDF/B-VIII, JEFF-3.1 and JENDL-3.3. For many levels especially when  $\Gamma_n \gg \Gamma_\gamma$ , the best fit is extracted fixing the neutron width to the transmission values, while in few cases ( $\Gamma_\gamma \gg \Gamma_n$ ) the  $\gamma$ -width is fixed to its average value. Figure

1 shows an example of fitted resonances, the list of the resonance parameters and of the main nuclear quantities will be reported in a forthcoming paper [13].

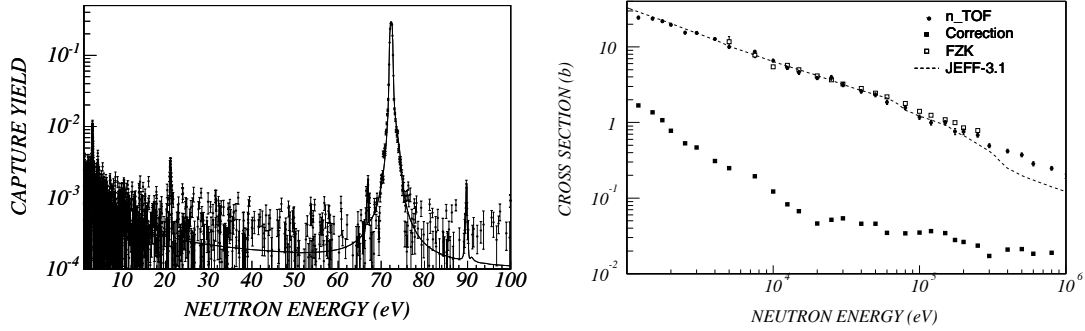


**Figure 1:** Left panel: the subtracted capture yield of the lanthanum sample is shown. The continuous curve represents the fit performed with SAMMY. Right panel: the  $^{151}\text{Sm}(n,\gamma)$  cross section in the unresolved resonance region is compared with the recent measurement at FZK [18] and with the JEFF-3.1 data (dashed line). The corrections for isotopic impurities, self-shielding and multiple scattering are also indicated.

The  $^{151}\text{Sm}(n,\gamma)$  cross section is calculated up to 1 keV by means of the resonance parameters, while between 1 keV and 1 MeV, the average cross section is provided [7], see Figure 1. All the levels are assumed to be  $s$ -waves and the main nuclear quantities are indicated as  $D_0 = 1.49 \pm 0.07$  eV  $S_0 = (3.87 \pm 0.33) \times 10^{-4}$ . The total accuracy for the  $^{151}\text{Sm}$  is estimated on average within the 6% and is mainly dominated by two systematical errors: neutron flux and PHWT and by statistical contribution. In the case of lanthanum the average uncertainty is around the 7% because of larger statistical contribution. According to the new capture cross section, the Maxwellian-averaged cross section (MACS) of both isotopes are accurately calculated. It is noticed that the MACS of  $^{139}\text{La}$  is in agreement with the recent activation measurements performed at Karlsruhe [14-15] while they are much smaller than the MACS estimated by the previous capture measurement [4]. Concerning the  $^{151}\text{Sm}$ , the previous estimations were based on the statistical model calculations and indicated a value at the temperature  $kT = 30$  keV between 1.50 and 2.80 barn while the present estimation based on the n\_TOF data indicates a value of 3.08 barn.

Including the MACS calculated in the present work in the Thermally Pulsing Asymptotic Giant Branch model [16], the *main* component of the  $s$  process makes 74.2% of the lanthanum solar abundance, about the same value estimated in O'Brien *et al.* (76.9%) [14] and in Winckler *et al.* [15] (70.0%), but higher than in Arlandini *et al.* [17] (64.2%) who used older and higher values for the MACS. Once the  $s$ -process abundance is accurately determined with respect to the solar lanthanum, the  $r$ -process contribution is completely fixed by its residual ( $N_r = 1 - N_s$ ). This estimation is extremely important for the understanding of chemically unevolved stars in the Galactic halo where the heavy elements are essentially provided by short-lived massive stars through the  $r$  process as indicated in Figure 2.

For the  $^{151}\text{Sm}$ , the investigated stellar model predicts an  $s$  process production of 78% for  $^{152}\text{Gd}$ , 91% for  $^{154}\text{Gd}$  with respect to the solar abundances, see Table 1. Compared to the previous analysis [17] we obtain an 10% higher and a 4% lower abundance for  $^{152}\text{Gd}$  and  $^{154}\text{Gd}$ ,

respectively. The missing fraction of the  $^{152}\text{Gd}$  abundance can in principle be accounted for by a 22% contribution from the  $p$ -process, consistent with the abundances of the closest  $p$ -only isotopes  $^{144}\text{Sm}$ ,  $^{156}\text{Dy}$  and  $^{158}\text{Dy}$  (for a discussion see the Ref. Wisshak *et al.* [18]). It is important to note that the theoretical stellar models of the  $p$  process predict a  $\sim 12\%$  contribution to the solar  $^{152}\text{Gd}$  abundance [19]. To investigate possible variations within the present AGB models, the stellar enhancement factor [20] and the  $\beta$ -decay rate were changed within plausible limits. The results of this sensitivity analysis are summarized in Table 1 where the standard case is listed in the second column. Variation of the  $\beta$ -decay rate and the MACS of  $^{151}\text{Sm}$  by 50% and 10%, respectively, gives obviously rise to a significant enhancement of the  $^{152}\text{Gd}$  abundance or even to an overproduction of this isotope. In contrast, variations of the  $\beta$ -decay rate and or the MACS of  $^{153}\text{Sm}$  affect only the small  $s$ -process contribution of  $^{154}\text{Sm}$  but do not contribute to the europium or gadolinium production. Similar changes of the parameters for  $^{152}\text{Eu}$  have no global effects on the final isotopic abundances. The last two columns of Table 1 are dealing with the  $s$  abundance of  $^{154}\text{Gd}$ , which is not fully accounted for. This deficiency can not be compensated by the  $p$  process, which is contributing only  $\leq 2\%$  to the abundance of  $^{154}\text{Gd}$ . Since the cross section of the unstable branch point  $^{154}\text{Eu}$  is obtained from statistical model calculations the 30% variation is certainly justified and almost sufficient to fully reproduce the missing  $^{154}\text{Gd}$  abundance.

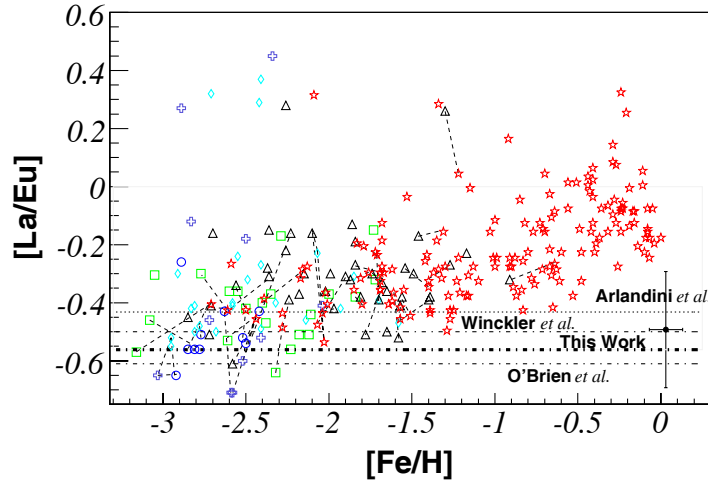


**Figure 2:** The spectroscopic ratio of the lanthanum with respect to the Europium as a function of the metallicity. The symbols indicate the spectroscopic ratio of several set of stars [13]. The dot-dashed line indicates the  $r$ -process contribution to the ratio calculated according to the TP-AGB model [16] and the MACS estimated with the n\_TOF data. The dashed line indicates the  $r$ -process contribution estimated in Ref. [14-15] while the dotted line represents the same quantity calculated according to Arlandini *et al.* [17]. The stars having  $[\text{La}/\text{Eu}] > 0.2$  represent the  $s$ -process rich stars and require of different treatment.

#### 4. Conclusion

The  $(n,\gamma)$  cross section of the  $^{139}\text{La}$  and  $^{151}\text{Sm}$  has been measured over a wide range of neutron energies using the n\_TOF facility at CERN. The reliability of the measurement and the accuracy of the results have been demonstrated by a complete presentation of the data analysis. The obtained physical quantities, i.e. resonance parameters, resonance integral, level densities,

neutron strength function, and average gamma widths, were found consistent with but significantly more accurate than previous results. The implications of the present results were discussed with respect mainly to nuclear astrophysics.

This work was supported partly by the EC under contract FIKW-CT-2000-00107 and by the funding agencies of the participating institutes.

**Table 1:** Sensitivity of  $s$ -process production factors for the average 1.5 and 3 solar mass AGB models of half the solar metallicity with respect to remaining nuclear physics uncertainties (all values relative to the  $s$ -only isotope  $^{150}\text{Sm}$ ). The largest variations are indicated in bold face.

Isotope	Standard	$\lambda_{\beta}(^{151}\text{Sm})$	$\langle\sigma\rangle(^{151}\text{Sm})$	$\langle\sigma\rangle(^{153}\text{Eu})$	$\lambda_{\beta}(^{153}\text{Sm})$	$\langle\sigma\rangle(^{154}\text{Eu})$	$\lambda_{\beta}(^{154}\text{Eu})$
		$\times 1.5$	$\times 0.9$	$\times 1.1$	$\times 1.5$	$\times 0.7$	$\times 1.5$
$^{150}\text{Sm}$	1	1	1	1	1	1	1
$^{152}\text{Sm}$	0.226	0.222	0.225	0.226	0.226	0.226	0.226
$^{154}\text{Sm}$	0.025	0.025	0.025	0.025	<b>0.018</b>	0.025	0.025
$^{151}\text{Eu}$	0.058	0.057	<b>0.063</b>	0.058	0.058	0.058	0.058
$^{153}\text{Eu}$	0.057	0.057	0.057	<b>0.052</b>	0.057	0.057	0.057
$^{152}\text{Gd}$	0.781	<b>1.105</b>	<b>0.852</b>	0.781	0.781	0.781	0.781
$^{154}\text{Gd}$	0.909	0.911	0.909	0.910	0.910	<b>0.957</b>	<b>0.944</b>

## References

- [1] F. Käppeler, *Progress in Nuclear and Particle Physics* **43**, 419 (1999).
- [2] N. J. Pattenden, *Nuclear Science and Engineering* **17**, 371 (1963).
- [3] G.J. Kirouac and H.M. Eiland, *Physical Review C* **11**, 895 (1975).
- [4] L. Musgrove, B. J. Allen, and R. L. Macklin, *Australian Journal of Physics* **30**, 599 (1977).
- [5] Y. Nakajima *et al.*, *Journal of Nuclear Science and Technology* **20**, 183 (1983).
- [6] G. Hacken, J. Rainwater, H. I. Liou, and U. N. Singh, *Physical Review C* **13**, 5 (1976).
- [7] S. Marrone *et al.*, *Physical Review C* **73**, 034604 (2006).
- [8] S. Marrone *et al.*, *Nuclear Instruments and Methods A* **517**, 389 (2004).
- [9] R. Plag *et al.*, *Nuclear Instruments and Methods A* **496**, 425 (2003).
- [10] U. Abbondanno *et al.*, *Nuclear Instruments and Methods A* **538**, 692 (2005).
- [11] S. Marrone *et al.*, *Nuclear Instruments and Methods A* **490**, 299 (2002).
- [12] U. Abbondanno *et al.*, *Nuclear Instruments and Methods A* **538**, 692 (2004).
- [13] R. Terlizzi *et al.*, paper in preparation.
- [14] S. O'Brien *et al.*, *Physical Review C* **68**, 35801 (2003).
- [15] N. Winckler *et al.*, in print on the *The Astrophysical Journal*.
- [16] Busso, Gallino, and Wasserburg, *Annual Review of Astronomy and Astrophysics* **37**, 239 (1999).
- [17] C. Arlandini *et al.*, *The Astrophysical Journal* **525**, 886 (1999).
- [18] K. Wisshak *et al.*, *Physical Review C* **73**, 015802 (2006).
- [19] T. Rauscher *et al.*, *The Astrophysical Journal* **576**, 323 (2002).
- [20] Z.Y. Bao *et al.*, *Atomic Data and Nuclear Data Tables* **76**, 70 (2000).